Influence of phase transition on sloshing impact pressures described by a generalized Bagnold's model

Matthieu Ancellin[(1)], Laurent Brosset[(2)], Jean-Michel Ghidaglia[(1)]
[1]Centre de Mathématiques et de Leurs Applications, Ecole Normale Supérieure de Cachan and CNRS, Cachan, France
[2]GTT (Gaztransport & Technigaz), Saint-Rémy-lès-Chevreuse, France

ABSTRACT

The effect of phase transition during liquid impacts involving entrapped gas pockets might play an important role for fluids close to thermodynamic equilibrium as LNG/NG in tanks of LNG carriers. However, this role is disregarded during Sloshing Model Tests. This issue was addressed in Braeunig et al. (2010) by introducing a simple 1D piston model. The phase transition between the liquid and its vapor was described through a simple quasi-static relaxation model including thermal exchanges at the wall.

A more advanced version of this 1D model is presented. A thermodynamic description of the relaxation process from unbalanced conditions to the liquid/vapor equilibrium is proposed. The new model conserves the total energy of the liquid-vapor system. It generalizes the classical Bagnold's model (1939) and can be formulated in dimensionless form exhibiting not only the usual Impact number (Bagnold) and numbers related to thermo-dynamic properties of the fluid (thermal capacities, latent heat), but also characteristic times for respectively mass transfer and energy transfer.

The model shows that, as observed experimentally (sloshing model tests with water and steam described by Maillard et al., 2009), phase transition mitigates pressure impacts involving entrapped gas and damps drastically the oscillations of the gas pockets. The amplitudes of mitigation and of damping depend on the fluid properties.

KEY WORDS: sloshing, LNG, phase transition, condensation, model test, scaling law, Bagnold, dimensionless number, compressibility.

NOMENCLATURE

Symbol	Unit	Meaning
e	*J*	Internal energy of the vapor
E	*J*	Total internal energy (vapor and liquid)
n	*mol*	Number of moles of the vapor
N	*mol*	Total number of moles (vapor and liquid)
z	*m*	Vertical coordinate of the piston (origin at the bottom of the chamber, axis pointing upward)
T_i	*K*	Temperature of phase i*
P_g	*Pa*	Pressure in the vapor
P_u	*Pa*	Ullage pressure
ρ_i	$kg.m^{-3}$	Density of phase i*
H_g	$J.mol^{-1}$	Molar enthalpy of phase the vapor
R	$J.mol^{-1}K^{-1}$	Perfect gas constant
L_{vap}, H_{vap}	$J.mol^{-1}$	Latent heat and latent enthalpy (evaporation)
C_i	$J.mol^{-1}K^{-1}$	Isochoric thermal capacity of phase i*
M	$kg.mol^{-1}$	Molar mass
$P_{sat}(T)$	*Pa*	Saturation curve
A, B, C	*None, K, K*	Coefficients in Antoine's law
Φ_μ	$mol.m^{-2}.s^{-1}$	Flux of mass exchanged between the two phases
Φ_q	$J.m^{-2}.s^{-1}$	Flux of energy exchanged between the two phases
$L_{\mu\mu}$	$mol^2.K.J^{-1}.s^{-1}m^{-2}$	Onsager's coefficient
$L_{q\mu}$	$mol.K.s^{-1}.m^{-2}$	Onsager's coefficient
L_{qq}	$kg.K.s^{-3}$	Onsager's coefficient
M_{piston}	*kg*	Mass of the piston
DR	-	Density ratio ρ_g/ρ_l between gas and liquid

**i=l for liquid phase, i=g for vapor phase*

INTRODUCTION

Context

Today, sloshing model tests, most of the time at scale 1:40, are considered as the only relevant tool for any sloshing assessment of a real project of LNG carrier (see Gervaise et al., 2009). The model tank motions are imposed by a six degree-of-freedom rig after down-scaling full scale calculated ship motions. The motion down-scaling is obtained by applying a coefficient $1/\lambda$ (geometrical scale) on the amplitudes and a coefficient $1/\sqrt{\lambda}$ on the times, namely by keeping Froude number the same at both scales. Doing so does not imply that the flow at model scale is completely Froude-similar as the flow at Froude scale and that measured impact pressures can simply be up-scaled from the tests to full scale by Froude similarity. Indeed some physical phenomena occur during the impacts at full scale and not at model scale (e.g. phase transition and fluid-structure interactions) and some physical phenomena occur at both scales but differently because the fluid properties are not relevantly scaled (e.g. the compressibility of the gas and of the liquid and the surface tension between liquid and gas).

As the density ratio DR between the gas and the liquid is kept the same at both scales (use of a heavy gas during the tests), the global flows are assumed to be statistically Froude- similar at both scales. This means that any possible local inflow condition for an impact at full scale is assumed to find a Froude similar inflow condition at model scale with the same probability of occurrence. Nevertheless, for Froude-similar inflow conditions at both scales the local phenomena will bias the Froude similarity during any impact. For the time being, GTT developed a know-how based on the feedback from the LNG carrier fleet in order to derive appropriate statistical scaling factors. At the same time a research work is carried out to define a more direct approach. This implies a better understanding of the scaling biases in order both to improve the experimental modeling (better representativeness of sloshing model tests) and to be able to scale adequately the biased experimental results.

Elementary Loading Processes (ELP)

Scaling impact pressures from sloshing model tests to the full scale of an LNG carrier implies being able to decompose all the loading components for any liquid impact on the walls and evaluate their relative importance at both scales. This question has been addressed by Brosset et al. (2011) by analyzing a single breaking wave impact on a wall, thanks to the concept of Elementary Loading Process (ELP) described in detail in Lafeber et al. (2012a).

The loads induced by any breaking wave impact and more generally by any liquid impact on a wall are time and space distributions that are considered as a combination of only three components:

- ELP1: *Direct impact* due to the discontinuity of velocity imposed by the wall to the liquid particles. This ELP is associated to the liquid compressibility (pressure waves) and the elasticity of the wall (strain waves). It leads to very sharp pressure peaks that are difficult to detect experimentally.
- ELP2: *Building jet*. This is simply the hydrodynamic load associated to the change of momentum imposed by the wall to the flow. It is significant only at the root of the jets building along the wall just after the contact. The pressure signature is a travelling pulse which can be very sharp in some conditions like Flip-Through impacts.
- ELP3: *Compression/expansion of gas* while escaping or when entrapped. This ELP is associated to the compressibility of the gas. It is characterized by pressure oscillations, at least when no phase transition is involved.

Other physical phenomena involved during a liquid impact (e.g. phase transition or fluid-structure interaction, development of free surface instabilities) modify the development of these ELPs and therefore influence the resulting load. Nevertheless they do not have their own related ELP. The most typical combination of ELPs, as determined from many wave impact tests in flumes, was summarized in a simple chart by Lafeber et al. (2012a). The possible associated physical phenomena are included in the chart. This chart is shown in **Figure 1**.

Each of these ELPs considered separately follows a different similarity law. The main problem for scaling is therefore due to the interactions between them. GTT's strategy consists in studying at different scales relevant scenarios staging more and more complex combinations of ELPs and associated physical phenomena. The most simple scenarios are those involving a single ELP through a so-called *canonical model*: flat impact of a column of liquid without gas for ELP1, as studied numerically e.g. by Couty et al. (2000); drop test of a wedge on a liquid at rest for ELP2, as studied experimentally by Zhao et al. (1993); piston problem as studied analytically by Bagnold (1939) for ELP3.

The scenarios are studied either by relevant experiments (Lafeber et al., 2012b) or numerical simulations (Braeunig et al., 2009, Guilcher et al., 2012) or semi-analytical developments (Braeunig et al., 2010).

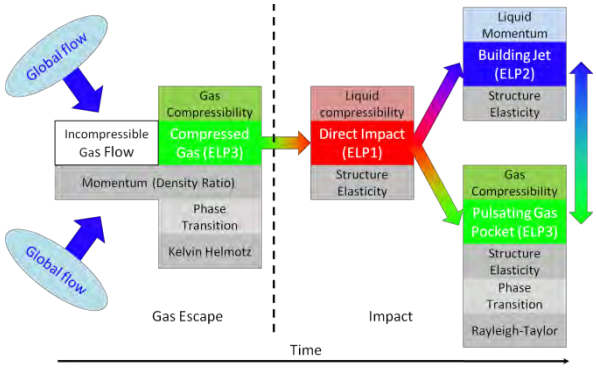

Figure 1 - Typical combination of ELPs - Associated physical phenomena (from Lafeber et al., 2012a).

Influence of phase transition on sloshing loads

Phase transition is naturally included in the impact chart of **Figure 1**, associated with ELP3. It could change drastically the load generated by the gas compression. Yet, it has not been studied much in the context of liquid impacts as sloshing impacts within LNG tanks. Maillard et al. (2009) described sloshing model tests performed in a pressure vessel enabling testing water and its vapour along the phase boundary. The tests were restricted to high fill levels and especially designed to study the influence of DR, but some interesting results were also found related to the influence of phase transition, when comparing results obtained with water and vapour to results in the same conditions but with water and a non condensable gas at the same DR.

The statistical pressures proved to be slightly but significantly reduced when phase transition was possible, but only for high density ratios when the rate of entrapped gas pockets is high.

Another interesting result was mentioned: the pressure signatures of entrapped gas pockets were completely different when vapour was involved than when non condensable gas was involved, as shown in **Figure 2**. In both cases, the presence of gas pockets was simply identified because several neighbour sensors recorded exactly the same signal. Moreover the rates of entrapped gas-pockets in the corners were similar as DR was the same. Nevertheless, the typical pressure oscillations for any non condensable gas pocket were replaced by a single pressure peak for any vapour pocket. The oscillations were always so much damped that they could hardly be noticed.

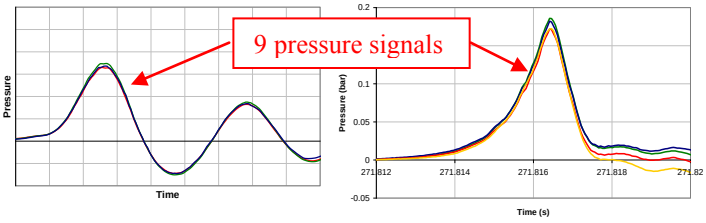

Water with non-condensable gas *Water with vapor along the phase boundary*

Figure 2 - Pressure signature for a gas pocket impact during sloshing model tests (from Maillard et al, 2009).

Such influence of the phase transition happens during a period corresponding to a sloshing pressure pulse. The order of magnitude of the duration is 1 ms at small scale. The dynamics of the condensation is

therefore supposed to play an important role.

Presentation of the work

This paper presents a *semi-analytical model* which is an extension of the piston model of Bagnold including the energy and mass transfers between two phases of the same fluid. The scenario studied is therefore the *canonical model of ELP3* when modified by the *phase transition phenomenon*. It is schematically represented in **Figure 3**.

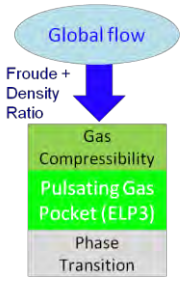

Figure 3 - Schematic representation of the studied scenario.

Bagnold model already proved to be very relevant for explaining the scaling of gas pocket pressures when entrapped during wave impacts at different scales (see Bogaert et al., 2010, Kimmoun et al., 2010 and Lafeber et al., 2012b).

The solution can be described in a dimensionless form using a unique dimensionless number S, called impact number, representing the intensity of the impact.

A first attempt was made by Braeunig et al. (2010), to develop an extension of the Bagnold model with phase transition. This model showed interesting trends, matching qualitatively those described in Maillard et al (2009) and recalled in the previous sub-section for sloshing vapor tests. Nevertheless it was based on too simple assumptions to allow a robust use in a large enough range of parameters. For example it did not conserve the energy and as it was based on a quasi-static approach (mechanical stage + forced return to the equilibrium at each time step), it did not describe the dynamic process leading from unbalanced condition to a new thermodynamic equilibrium.

The new model presented in this paper is based on Non Equilibrium Thermodynamics (NET). Characteristic times for thermal transfer and mass transfer between the two phases of the fluid will be exhibited. Initial Bagnold model will therefore be modified according to the ratio between these time characteristics and the impact duration.

EXTENSION OF THE BAGNOLD PISTON PROBLEM TO PHASE TRANSITION

Some of the different parameters used in the following sections are not defined directly in the text. The reader is invited to look at the nomenclature for definitions. See Ancellin (2011) for more details on the problem and its resolution.

Reference problem description

We consider a vertical tank with a constant internal section. A piston can slide vertically inside the tank. The chamber below the piston is filled by a pure fluid under both liquid and gas phases. The space above the piston is open and keeps a constant ullage pressure P_u. **Figure 4** shows a schematic representation of the problem.

The *main* parameters of the problem are:

- *n,* number of moles of the vapor
- *N,* total number of moles (liquid + vapor*)*
- *e,* internal energy of the vapor
- *E,* total internal energy(liquid + vapor)
- *z*, vertical coordinate of the piston (origin at the bottom of the chamber, axis pointing upwards)

The masses of the vapor and liquid phases are deduced from *n* and *N* thanks to the molar mass *M*. The liquid height is therefore:

$$b(e,n,E,N,z) = \frac{(N-n)M}{\rho_l} \qquad (1)$$

The gaseous phase is assumed as a perfect gas. Therefore the vapor pressure P_g is expressed by:

$$P_g(e,n,E,N,z) = nR\frac{T_g(e,n)}{z-b(e,n)} \qquad (2)$$

Actually *E* and *e* are variations of energy around a reference state defined by molar energies of the gas ε^g_{ref} and of the liquid ε^g_{ref} at temperature T_{ref}. This reference state might be either the initial or the final state. It might be at the thermodynamic equilibrium or not.

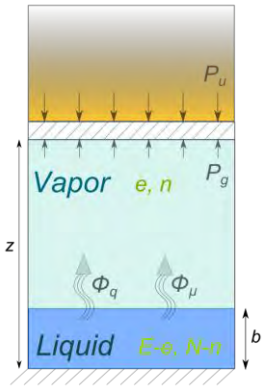

Figure 4 – Schematic representation of the piston problem with phase changes

Temperatures in the gas and in the liquid are therefore:

$$T_g(e,n,E,N,z) = T_{ref} + \frac{1}{C_g}\left(\frac{e}{n} - \varepsilon^g_{ref}\right) \qquad (3)$$

$$T_l(e,n,E,N,z) = T_{ref} + \frac{1}{C_l}\left(\frac{E-e}{N-n} - \varepsilon^l_{ref}\right) \qquad (4)$$

The problem could be expressed equivalently in terms of molar enthalpy of the gas and of the liquid.

Initial conditions of the problem are given by initial values of *n, N, e, E, z, ż* denoted respectively n_0, N, e_0, E_0,z_0, $\dot{z}_0$ with $\dot{z}$ and $\dot{z}_0$ respectively the vertical speed of the piston and its initial value.

A thermodynamic imbalance is created either from the initial state or from the compression of the gas due to the piston motion. There is therefore a flux of energy Φ_q and a flux of mass Φ_μ exchanged between the two phases until the return to the equilibrium, defined by a saturation curve $P_{sat}(T)$ in the pressure-temperature (P, T) diagram. $P_{sat}(T)$ is assumed to follow Antoine's law:

$$P_{sat}(T) = P_{atm}exp\left(A - \frac{B}{T-C}\right) \qquad (5)$$

with A, B, C depending on the fluid in the chamber.

Alternatively, Clapeyron's formula will be used in the vicinity of a point (P_{ref}, T_{ref}) at the equilibrium:

$$P_{sat}(T) = P_{ref}exp\left(\frac{H_{vap}}{R}\left(\frac{1}{T_{ref}} - \frac{1}{T}\right)\right) \qquad (6)$$

Like Bagnold's problem, this extended problem is assumed as a 1D problem: every parameter keeps the same value at a given *z* and all extensive parameters are defined with regard to a surface unit. Gravity is disregarded. Extension is trivial.

Theoretical model in dimensional form

The ordinary differential equations that describe the evolution of the system are :

$$\frac{de}{dt} = \Phi_q(e,n,E,N,z) - P_g(e,n,E,N,z)\frac{dz}{dt} \qquad (7)$$

$$\frac{dn}{dt} = \Phi_\mu(e,n,E,N,z) \qquad (8)$$

$$\frac{dE}{dt} = -P_g(e,n,E,N,z)\frac{dz}{dt} \qquad (9)$$

$$\frac{dN}{dt} = 0 \qquad (10)$$

$$\frac{d^2z}{dt^2} = \frac{P_g(e,n,E,N,z) - P_u}{M_{piston}}. \quad (11)$$

The meaning of these equations is as follows: (7) evolution of the energy of the vapor, (8) evolution of the mass of the vapor, (9) Evolution of the total energy of the substance, (10) Conservation of total mass, (11) fundamental principle of dynamics applied to the piston without gravity.

The power provided by the piston when moving is $(P_g - P_u)\frac{dz}{dt}$. The term $P_g \frac{dz}{dt}$ that appears in equations (7) and (9) represents only the share exchanged with the gas in the chamber.

In Non Equilibrium Thermodynamics (NET), see e.g. Lebon et al. (2008), the fluxes of energy Φ_q and mass Φ_μ vanish when the thermodynamic equilibrium is reached *i.e.* on the saturation curve. These fluxes can be explicitly expressed as follows:

$$\Phi_q = L_{qq}\Gamma_q + L_{q\mu}\Gamma_\mu \quad (12); \qquad \Phi_\mu = L_{q\mu}\Gamma_q + L_{\mu\mu}\Gamma_\mu \quad (13)$$

$\Gamma_q = \frac{1}{T_g} - \frac{1}{T_l}$ and $\Gamma_\mu = \frac{\mu_g}{T_g} - \frac{\mu_l}{T_l}$ being the *thermodynamic forces*, with μ_g and μ_g the chemical potential of respectively the gas and the liquid.

The thermodynamic forces can eventually be expressed as:

$$\Gamma_q = \frac{1}{T_{ref} + \frac{e}{nC_g}} - \frac{1}{T_{ref} + \frac{1}{C_l}\left(\frac{E-e}{N-n} + L_{vap}\right)} \quad (14)$$

$$\Gamma_\mu = R\, ln\left[\frac{P_{sat}\left[T_{ref} + \frac{1}{C_l}\left(\frac{E-e}{N-n} + L_{vap}\right)\right]\left(z - \frac{(N-n)M}{\rho_l}\right)}{nR\left(T_{ref} + \frac{e}{nC_g}\right)}\right] \quad (15)$$

It remains to define Onsager's coefficients L_{qq}, $L_{\mu\mu}$ and $L_{q\mu}$, which is not an easy task. In practice, they are expressed from the so-called resistances R_{qq}, $R_{\mu\mu}$ and $R_{q\mu}$ through simple algebraic relations (see *Ancellin* (2011)). Kinetic theory of gases allows to find analytical expressions for the $R_{\alpha\beta}$ for a mono-atomic gas in the vicinity of its triple point (see e.g. Bedeaux and Kjelstrup (1999)). Since we are neither considering mono-atomic gas nor states close to the triple point, we shall only retain from these expressions the order of magnitude for Onsager's coefficients $L_{\alpha\beta}$. A sensibility study with respect to the value of these coefficients will therefore be addressed later in this paper.

Theoretical model in dimensionless form

From $z_0, \dot{z}_0$ and the time *t*, we can define a dimensionless time $\tau = \omega t$, with $\omega = \frac{\dot{z}_0}{z_0}$.

In the same way we define the dimensionless variables ε, η, ν, ζ, ϑ corresponding respectively to *e, E, n, z, ż* by:

$e(t) = N\, L_{vap}\varepsilon(\tau)$, $E(t) = NL_{vap}\eta(\tau)$, $n(t) = N\nu(\tau)$, $z(t) = z_0\zeta(\tau)$ and $\dot{z}(t) = \dot{z}_0\,\vartheta(\tau)$.

The initial conditions of the problem become:

$\varepsilon(0) = 0$, $\eta(0) = \nu_0 - 1$, $\nu(0) = \nu_0$, $\zeta(0) = 1$, $\vartheta(0) = -1$ with $\nu_0 = \frac{n_0}{N}$ the initial gas fraction.

Dimensionless temperatures in the gas and in the liquid and dimensionless pressure in the gas are also defined by reference to their respective initial values : $T_g{}^* = \frac{T_g}{T_{g_0}}$, $T_l{}^* = \frac{T_l}{T_{l_0}}$, $P_g{}^* = \frac{P_g}{P_0}$.

After some simplifications/linearizations of the problem, including setting to zero the coupling Onsager's coefficient $L_{q\mu}$ (this point will be justified later) and using Clapeyron's formula (6) for defining the saturation curve, the equations (7), (8), (9), (10), (11) become:

$$\frac{d\varepsilon}{d\tau} = \Omega_e\left(\frac{\eta-\varepsilon}{1-\nu} + 1 - \frac{\kappa_l}{\kappa_g}\frac{\varepsilon}{\nu}\right) + \left(\frac{\varepsilon}{\nu}\left(1 + \frac{1}{\kappa_g}\right) + \frac{1}{\Lambda}\right)\frac{d\nu}{d\tau} + \frac{d\eta}{d\tau} \quad (16)$$

$$\frac{d\eta}{d\tau} = -\frac{1}{\Lambda}\frac{\nu + \frac{\Lambda}{\kappa_g}\varepsilon}{\varsigma}\,\vartheta \quad (17)$$

$$\frac{d\nu}{d\tau} = \Omega_n\left[ln\left(\frac{\nu_0\zeta}{\nu + \frac{\Lambda}{\kappa_g}\varepsilon}\right) + \frac{\Lambda^2}{\kappa_l}\left(\frac{\eta-\epsilon}{1-\nu} + 1\right)\right] \quad (18)$$

$$\frac{d\varsigma}{d\tau} = \vartheta \quad (19)$$

$$\frac{d\vartheta}{d\tau} = \frac{1}{S}\left(\frac{\nu + \frac{\Lambda}{\kappa_g}\varepsilon}{\nu_0\zeta} - 1\right). \quad (20)$$

This exhibits some dimensionless numbers:

$\kappa_g = \frac{C_g}{R}$, $\kappa_l = \frac{C_l}{R}$, $\Lambda = \frac{L_{vap}}{RT_0}$ are related to the fluid properties;

$\Omega_e = \frac{\nu_0 L_{qq}}{T_0 P_0 z_0 \kappa_l}\frac{1}{\omega}$, $\Omega_n = \frac{T_0 R^2 L_{\mu\mu}}{P_0 z_0}\frac{1}{\omega}$ can be considered as characteristic dimensionless frequencies respectively related to the energy transfer and the mass transfer;

$S = \frac{M_{piston}\dot{z_0}^2}{P_0 z_0}$ is the *impact number* appearing in the traditional Bagnold model (see Bogaert et al. (2010) and Kimmoun et al. (2010)).

Implementation

Two programs have been written in Matlab:

- *Program 1*: parameters are in dimensional form, the piston is fixed (z(t)=z$_0$), Initial conditions for gas and liquid phases are out of the thermodynamic equilibrium, Onsager's transport coefficients L_{qq}, $L_{\mu\mu}$, $L_{q\mu}$ are calculated according to kinetic theory of gases;
- *Program 2*: parameters are in dimensionless form, the piston has an initial velocity. Initial conditions are in thermodynamic equilibrium. Onsager's transport coefficients L_{qq} and $L_{\mu\mu}$ are assumed as constants: $L_{qq} = 10^9$ kg K s^{-3}, $L_{\mu\mu} = 1$ mol^2 K J^{-1} s^{-1}m^{-2} for water and $L_{qq} = 10^9$ kg K s^{-3}, $L_{\mu\mu} = 100$ mol^2 K J^{-1} s^{-1}m^{-2} for methane. As even the order of magnitude of these values is uncertain, their influence is studied in detail.

Bagnold's model corresponds to $\Phi_q = 0$ (no energy transfer) and $\Phi_\mu = 0$ (no mass transfer). It corresponds also to $\Omega_e = \Omega_n = 0$ when using the dimensionless model. The case of energy transfer between phases, without mass transfer ($\Phi_\mu = 0$) can also be studied with this model.

Properties of water and methane are shown in **Table 1**.

Table 1 – Properties of water and methane.

Quantity	Water	Methane
M ($kg.mol^{-1}$)	0.018	0.016
L_{vap} ($J.\ mol^{-1}$)	37 500	8 100
C_g ($JK^{-1}mol^{-1}$)	28	40
C_l ($JK^{-1}mol^{-1}$)	75	55
ρ_l ($kg.m^{-3}$)	1 000	416
P_{triple} (bar)	0.006	0.11
T_{triple} (K)	273	90
P_{critic} (bar)	220	46
T_{critic} (K)	647	190
A in P_{sat}	5.083	3.98
B (K) in P_{sat}	1 663.12	443
C (K) in P_{sat}	-45.62	-0.49

SENSITIVITY STUDIES

In this section, sensitivity studies are presented in order to show how the fluid manage to come back to a thermodynamic equilibrium starting from non-equilibrium conditions and also to check the influence of the Onsager's transport coefficients for the values of which a large uncertainty exists.

All results presented in this section have been obtained with *Program 1* for a fixed piston ($z_0 = 1\ m,\ \dot{z} = 0\ m/s$),.with water. In the different graphs, curves related to the gas behavior are plotted in red whilst curves related to the liquid are plotted in blue.

Influence of initial pressure P_0^g and temperature T_0^g in the gas: case 1

Initial temperature of the liquid is taken at $T_0^l = 370\ K$. Initial liquid fraction is fixed by $b_0 = 0.01$. With this initial liquid fraction, liquid phase represents 1% of the volume but 95% of the total mass.

4 x 4 initial conditions have been studied corresponding to pressures $P_0^g = 90, 100, 110, 120$ kPa and temperatures T_0^g varying from 362.5 K to 377.5 K by step of 5 K. Results are shown in **Figure 5** and **Figure 6**.

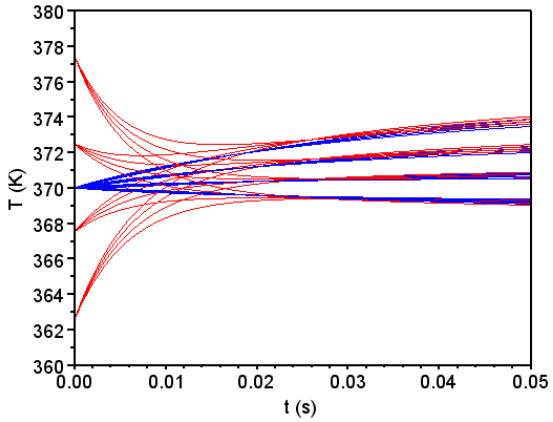

Figure 5 – Histories of temperatures in gas (red) and in liquid (blue) - 4 initial temperatures of gas ($T_0^g = 362.5, 367.5, 372.5, 377.5\ K$) and 4 initial pressures of gas ($P_0^g = 90, 100, 110, 120\ kPa$)
$z_0 = 1\ m,\ \dot{z} = 0,\ T_0^l = 370\ K, b_0 = 0.01$.

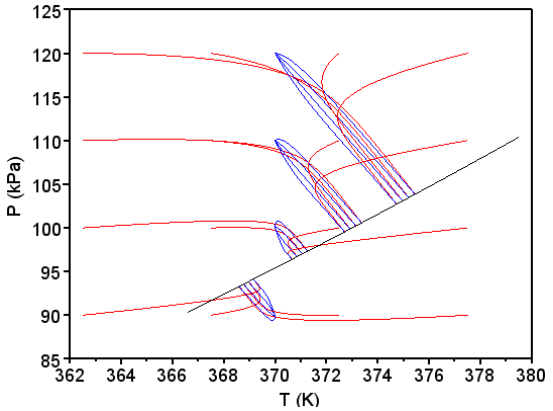

Figure 6 – Pressure vs. temperature in gas (red) and in liquid (blue) - 4 initial temperatures of gas ($T_0^g = 362.5, 367.5, 372.5, 377.5\ K$) and 4 initial pressures of gas ($P_0^g = 90, 100, 110, 120\ kPa$) - Saturation curve in grey - $z_0 = 1\ m,\ \dot{z} = 0,\ T_0^l = 370\ K, b_0 = 0.01$.

There are two different steps in the relaxation : the return to thermal equilibrium lasts about 25 ms. Afterwards, the temperatures and pressures of liquid and gas evolve similarly on the same side of the saturation curve in the (P, T) diagram, until the return to liquid-vapor equilibrium, which lasts about 200 ms for the conditions studied.

The four calculations with an initial pressure of 90 kPa lead to a final equilibrium through a vaporization process. All the other calculations correspond to a condensation process.

The final thermodynamic equilibrium is more influenced by the initial pressure than the initial temperature in the gas. A larger initial pressure leads to a larger final pressure for a large range of initial temperature. Surprisingly, for a fixed initial pressure, a larger initial temperature leads to a smaller final temperature whatever the initial pressure.

Influence of initial liquid fraction: case 2

Initial temperature of gas and liquid are respectively $T_0^g = 360$ K and $T_0^l = 380$ K. Initial pressure in the gas is $P_0^g = 100$ kPa.

Six initial liquid volume fractions and corresponding initial liquid mass fractions have been studied according to **Table 2**. The return to the equilibrium is shown in a (P, T) diagram represented in **Figure 7**.

Table 2 – Liquid volume fractions and mass fractions in calculations presented in **Figure 7**.

Curve index	Liquid volume fraction	Liquid mass fraction
a	13 %	99.5 %
b	1.8 %	97 %
c	0.24 %	80 %
d	0.034 %	35 %
e	0.0045 %	7 %
f	0.00061 %	1 %

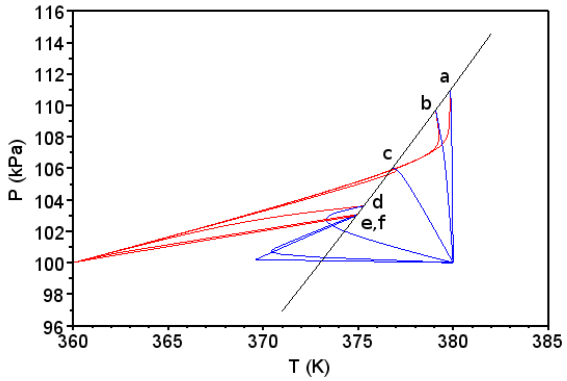

Figure 7 – Pressure vs. temperature in gas (red) and liquid (blue) for six different initial liquid volume fractions given in **Table 2** - Saturation curve in grey.
$z_0 = 1\ m,\ \dot{z} = 0,\ T_0^g = 360\ K, T_0^l = 380\ K, P_0^g = 100\ kPa$.

The six calculations start with the same imbalanced conditions with regards to the saturation curve but the final equilibrium depends strongly on the initial liquid fraction. Indeed the latent heat will influence differently the temperatures according to the quantity of liquid that will provide or gain it.

Two asymptotic cases can be observed:

- When there is a large fraction of liquid (cases ***a*** and ***b***), the liquid acts like a thermostat. The liquid temperature is very stable and fixes the final state. The gas pressure must increase together with its

temperature during eventually an evaporation process.

- When the initial liquid volume fraction is small (cases ***e*** and ***f***), the liquid temperature decreases first at constant pressure and afterwards increases together with its pressure. The turn between the two phases is very sharp and not intuitive.

Influence of Onsager's coupling coefficient $L_{q\mu}$

Ten calculations are made multiplying Onsager's coupling coefficient ${L_{q\mu}}^{ref}$ by a coefficient varying between 0 et 9, for initial conditions corresponding to $T_0^g = 370$ K, $T_0^l = 380$ K, $P_0^g = 100$ kPa, $b_0 = 0.01$ m, ${L_{q\mu}}^{ref}$ is calculated according to kinetic theory of gases. Results are shown in **Figure 8**.

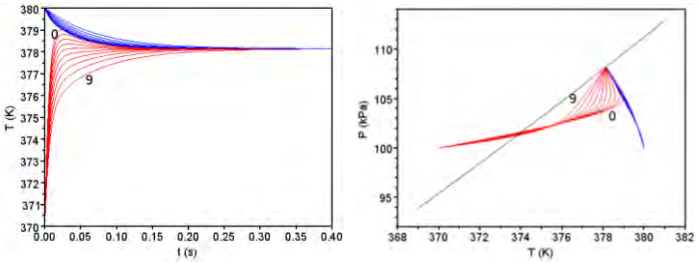

Histories of temperatures in gas (red) and liquid (blue)

Pressure vs. temperature in gas (red) and liquid (blue). Saturation curve in grey.

Figure 8 – Influence of Onsager's coupling coefficient. –
$L_{q\mu} = \alpha . {L_{q\mu}}^{ref}$ with α=0, 1,..., 9.
$z_0 = 1$ m, $\dot{z} = 0$, $T_0^g = 370\ K$, $T_0^l = 380\ K$, $P_0^g = 100$ kPa, $b_0 = 0.01$ m.

As expected coupling coefficients have no influence on the final state of equilibrium. For small coupling coefficient the thermal stage is more disconnected from the mass transfer stage. In that case, this last stage evolves for a large period of time with equal temperature and pressure in both phases. The results obtained with α=0 are very close to those obtained with α=1. This has been checked with other very different initial conditions.

Therefore, neglecting $L_{q\mu}$ in *Program 2* should not lead to noticeable different results than with *Program 1*. This does not mean that small values of the coupling coefficient are relevant.

Time evolution of Onsager's coefficients L_{qq}, $L_{\mu\mu}$ and $L_{q\mu}$

Program 1 takes into account Onsager's coefficients as determined at each time step by analytical expressions from kinetic theory of gases under the assumption of a mono-atomic gas in the vicinity of its triple point (see Bedeaux and Kjelstrup, 1999).

The time histories of the three coefficients for three calculations from case 1 (see **Figure 5** and **Figure 6**) are presented in **Figure 9** in terms of relative variations with regard to their initial values.

The three cases correspond to $(P_0^g, T_0^g) = (90\ kPa, 362.5\ K)$, $(P_0^g, T_0^g) = (100\ kPa, 372.5\ K)$ and $(P_0^g, T_0^g) = (110\ kPa, 372.5\ K)$ for $T_0^l = 370K, z_0 = 1\ m, b_0 = 0.01$ m. The three lines $L_{qq}(t)$, $L_{\mu\mu}(t)$ and $L_{q\mu}(t)$ are grouped for each case, which are respectively defined from top to bottom in the figure.

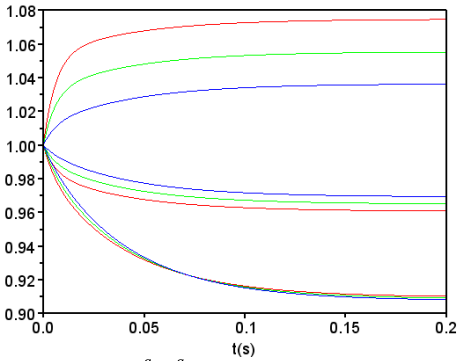

Top: $(P_0^g, T_0^g) = (90\ kPa, 362.5\ K)$
Centre: $(P_0^g, T_0^g) = (100\ kPa, 372.5\ K)$
Bottom: $(P_0^g, T_0^g) = (110\ kPa, 372.5\ K)$
$T_0^l = 370K, z_0 = 1\ m, b_0 = 0.01\ m$

Figure 9 – Relative time variations of Onsager's coefficients L_{qq} (red), $L_{\mu\mu}$ (blue) and $L_{q\mu}$ (green) with regard to their initial value.

The time histories of the three coefficients for three calculations from case 2 (see **Figure 7**) are presented in **Figure 10** in terms of relative variations with regard to their initial values. The cases correspond to gas fractions **a**, **c**, **e** in **Table 2**.

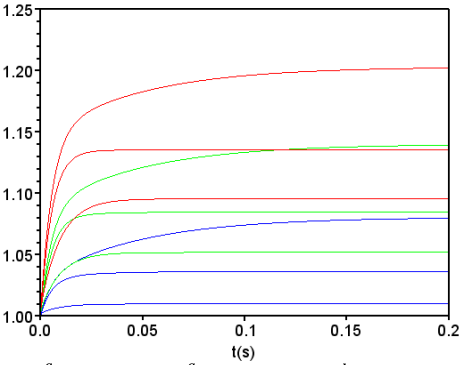

$P_0^g = 100\ kPa$, $T_0^g = 360\ K$, $T_0^l = 380\ K$
*Liquid fractions in **Table 2**– case 2 **a**, **c**, **e***

Figure 10 – Relative time variations of Onsager's coefficients L_{qq} (red), $L_{\mu\mu}$ (blue) and $L_{q\mu}$ (green) with regard to their initial value.

For the different relaxations from case 1, the three coefficients vary within [0.91, 1.075]. For case 2, they vary within [1.0, 1.19].

- L_{qq} is the largest coefficient and has also the largest variations (120% of its initial value). $L_{\mu\mu}$ is the smallest with also the smallest variations.
- Variations are more important for large liquid fractions (**a** > **c** > **e**).

The assumption of constant Onsager's coefficients makes the calculations much easier but might be sometimes not completely relevant. Now, the values for these assumed-constant-coefficients are also uncertain. The influence of these values is addressed in the next section.

COMPARISON WITH BAGNOLD MODEL

Bagnold's model (see Bagnold, 1939) can be written in a dimensionless form. A single dimensionless number, the impact number $S = \frac{M_{piston}\dot{z}_0^{\ 2}}{P_0 z_0}$, governs the behaviors of the piston and the gas chamber. S is representative of the violence of the impact: the larger S, the more violent the impact.

In this section, the results obtained with the extended model with phase

transition are compared with those obtained with the Bagnold model. *Program 2*, in dimensionless form, is used for the extended model.

First of all the influence of Onsager's coefficients, considered as constant versus time, is addressed, as the values to take for these constants are the most uncertain in the model. Afterwards, the influence of the initial liquid fraction is studied. Finally time histories are given for the main parameters including the pressure inside the gas chamber.

Influence of Ω_e and Ω_n

The values of Onsager's coefficients L_{qq} and $L_{\mu\mu}$.are disputed. Indeed, the discrepancies between different experimental results or between theoretical values (kinetic theory of gases) and experimental values can be important (see Fang et al. (1999), Bedeaux et al. (1999), Badam et al. (2007)).

The influence of these coefficients is studied, keeping the other parameters unchanged. The whole reasonable range of values is screened. Their variations induce directly the variations of Ω_e and Ω_n, the two dimensionless characteristic frequencies of respectively the thermal transfer and the mass transfer.

The results are presented for initial conditions corresponding on the one hand to water/vapor ($T_0^g = T_0^l = 373$ K, $P_0 = P_{Sat}(T_0) \approx 100$ kPa) and on the other hand to methane ($T_0^g = T_0^l = 111$ K, $P_0 = P_{Sat}(T_0) \approx 100$ kPa), both initially considered in thermodynamic equilibrium at atmospheric pressure. For both cases, impact conditions correspond to ω = 7.07 s^{-1}, S=0.5, $\nu_0 = 0.1$.

Results are presented in **Figure 11** in terms of dimensionless pressure P_g^*. As, after tests presented in Maillard et al., (2009), damping of the oscillations were expected, not only the first maximum pressure is displayed but also the maximum of the second peak, as a measure of the decay. Both pressures are presented as surfaces in the plane ($\log(\Omega_e)$, $\log(\Omega_n)$). The value obtained with Bagnold solution is presented as a plane $P_g^* = cte$, as reference. The three surfaces are superimposed in transparence.

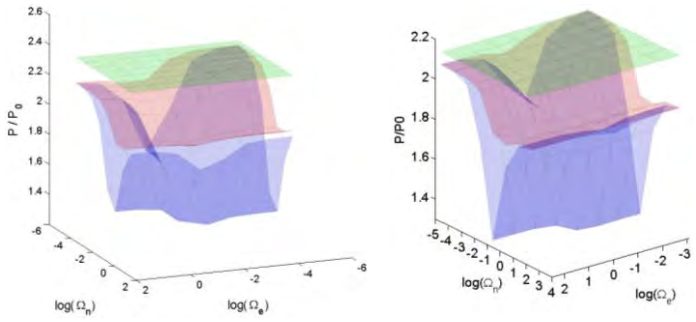

Water - $T_0^g = T_0^l = 373$ K Methane - $T_0^g = T_0^l = 111$ K

Figure 11 - Dimensionless pressure vs. Dimensionless energy transfer frequency Ω_e and dimensionless mass transfer frequency Ω_n.
Maximum pressure with Bagnold model (green)
Maximum pressure with phase transition model (pink)
Maximum second pressure peak with phase transition model (blue)
$\omega = 7.07$ s^{-1}, S=0.5, $\nu_0 = 0.1$, $P_0 \approx 100$ kPa.

For both fluids (water and methane), the results show a double resonance phenomenon: one related to the thermal transfer governed by Ω_e and one related to the mass transfer governed by Ω_n.

This means that there is a set of properties that is the most suited for a maximum energy transfer and there is a set of properties that is the most suited for a maximum mass transfer during the duration of the selected impact.

When Ω_e is small or when Ω_n is small, the thermal transfer or the mass transfer are too slow to have any influence during the impact. When both of them are small at the same time the results are the same as with Bagnold model.

According to the extended Bagnold's model, the first peak is always mitigated and the oscillations are always damped, whatever the values for L_{qq} and $L_{\mu\mu}$ taken in all the possible range for them. This is true for both water and methane. Depending on the values taken for L_{qq} and $L_{\mu\mu}$ and the resulting distance to both energy and mass transfer resonances, the mitigation will be more or less pronounced. The sloshing model vapor tests presented in Maillard et al. (2009) seem to prove that a very strong attenuation of the oscillations is actually possible with water.

Considering the large uncertainties on the data for defining Onsager's coefficients and as the trends for methane and water are the same, the results presented below refer only to water with $L_{qq} = 10^9$ kg K s^{-3} and $L_{\mu\mu} = 1$ mol^2 K J^{-1} s^{-1}m^{-2}.

Influence of the initial gas fraction

For any value of the initial volume gas fraction ν_0, we would like to obtain a modified Bagnold curve ${P_g^*}_{max}(S)$. Actually, it means that we need to build a surface ${P_g^*}_{max}(S, \nu_0)$ in the plane (S, ν_0). As we want not only to quantify a possible reduction or magnification of the maximum pressure inside the gas chamber but also quantify the damping of the oscillations, we would also like to obtain a second curve ${P_g^*}_{second\ max}$(S) corresponding to the maximum pressure during the second oscillation, therefore a second surface ${P_g^*}_{second\ max}$(S, ν_0).

Figure 12 presents the two surfaces plus a third surface defined from Bagnold curve ${P_{Bag}^*}_{max}(S)$ by ${P_{Bag}^*}_{max}(S, \nu_0) = {P_{Bag}^*}_{max}(S)$. The three surfaces are superimposed in transparence for initial conditions corresponding to water and vapor with $T_0^g = T_0^l = 373$ K, $P_0 = P_{Sat}(T_0) \approx 100$ kPa and with ω calculated from M_{Piston} = 1000 kg, z_0=1 m and S.

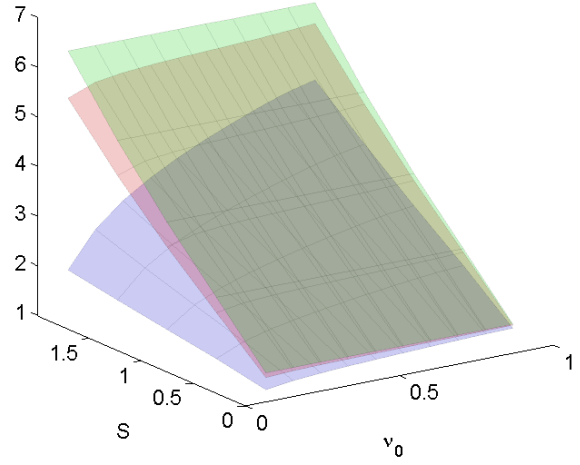

Figure 12 – Dimensionless pressure vs. inital gas fraction ν_0 and impact number S.
Maximum pressure with Bagnold model (green)
Maximum pressure with Phase transition model (pink)
Maximum second pressure peak with phase transition model (blue)
$T_0^g = T_0^l = 373$ K, $P_0 \approx 100$ kPa, $L_{qq} = 10^9$ kg K s^{-3}, $L_{\mu\mu} = 1$ mol^2 K J^{-1} s^{-1}m^{-2},
ω is calculated from M_{Piston} = 1000 kg, z_0=1 m and S.

Whatever the value of the initial gas fraction, the maximum pressure is reduced when energy and mass transfer are possible and the second maximum is reduced compared to the first. These two reductions are larger when the liquid fraction increases. The damping of the gas pocket oscillations can be very large when the liquid is dominant.

The limit cases displayed in **Figure 12** are for $\nu_0 = 0.1$ and $\nu_0 = 0.9$. For $\nu_0 = 0.1$, all the gas is transformed into liquid during the first compression and the piston reaches the bottom. For $\nu_0 = 0.9$, all the liquid evaporates during the first ascent of the piston.

These trends are exactly those that have been observed during sloshing model tests with water and vapor as described by Maillard et al. (2009). It is therefore, reasonable to consider that energy and mass transfers between phases are the causes for both the reduction of statistical pressure and the vanishing of pressure oscillations for gas pockets that have been reported. This comparison with the vapor tests will be addressed further with the pressure time histories in the next sub-section.

ν_0 is to be considered as the parameter that defines the quantity of liquid involved in the energy and mass transfers when the quantity of gas (volume of the entrapped pocket) is fixed. It is different from the impacting mass (piston mass in the Bagnold model). When a gas pocket is entrapped during a sloshing impact, the quantity of gas to consider is trivially defined. But, as for the impacting liquid mass, it is not easy to define the liquid mass involved in the thermodynamic transfers. Nevertheless, it seems reasonable to consider that this liquid mass is larger for impacts at high filling levels than for impacts at low filling levels in a LNG tank and that the liquid fraction is high. Actually, a possible improvement of the model could be to discriminate the liquid mass involved in the energy transfer from the liquid mass involved in the mass transfer.

Time histories of the parameters

With the Bagnold model, dimensionless elevation of the piston ζ and pressure P_g^* oscillate without any damping. The characteristics of the oscillations depend only on the impact number S. Obviously, with the Bagnold model the gas fraction ν remains constant.

Figure 13 shows the time histories for ζ, ν, P_g^*, for the following initial conditions corresponding to water and vapor: $T_0^g = T_0^l = 373$ K, $P_0^g \approx 100$ kPa and $\nu_0 = 0.1$, $S = 0.8$, $\omega = 8.9\ s^{-1}$.

For such a high impact number, Bagnold model (results in dashed lines on the figure) leads to periodic oscillations of the piston with quick drops corresponding to sharp pressure rises followed by slow ascents corresponding to smooth pressure relaxations with a minimum pressure below the initial pressure. With the extended model taking into account energy and mass transfers between the phases, the oscillations of the piston elevation and of the gas pressure appear to be strongly damped and the first peak pressure is reduced as observed during sloshing model tests with water and vapor described by Maillard et al. (2009).

Actually, the damping of the oscillations for entrapped gas pockets during the sloshing vapor tests (see **Figure 2**) is even more pronounced than in the calculated results when considering a liquid fraction of $\nu_0 = 0.1$. During the sloshing tests with vapor, for all the gas pockets entrapped, the oscillations vanished almost completely. This was obtained for high fillings, for impacts in the corners of the ceiling. Such vanishing of the oscillations can be obtained with the extended Bagnold model with very low values of ν_0 (around 0.05), namely very high liquid fractions.

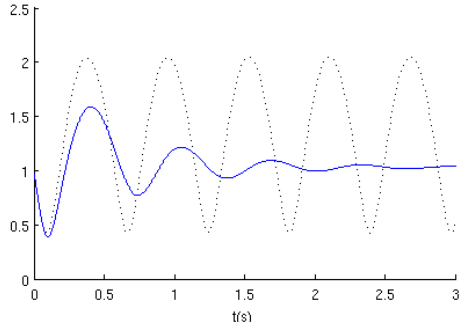

13.1 – History of the dimensionless elevation of the piston ζ

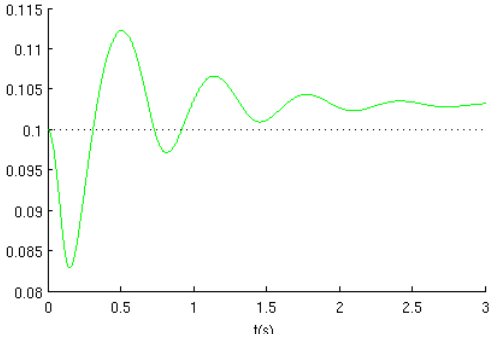

13.2 – History of the gas fraction ν

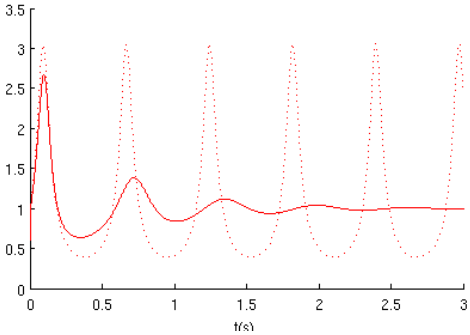

13.3 –History of the dimensionless pressure P_g^*

Figure 13 - Time histories for ζ (top), ν (middle), P_g^* (bottom) - $\nu_0 = 0.1$, $T_0^g = T_0^l = 373$ K, $P_0^g \approx 100$ kPa, $S = 0.8$, $\omega = 8.9\ s^{-1}$ $L_{qq} = 10^9$ kg K s^{-3}, $L_{\mu\mu} = 1$ mol^2 K J^{-1} s^{-1}m^{-2} - Bagnold results in dashed line.

The gas fraction presents also damped oscillations, starting by a strong drop (condensation). These oscillations are delayed compared to the pressure oscillations without phase transition because of the different time characteristics of the phenomena. This delay, brought by the energy transfer or/and the mass transfer between phases, explains the delay between the pressure curves. It is connected to the resonance phenomenon shown in **Figure 11** This delay is progressively gained, especially during each quick compression phases, as could be expected.

The final balance is positive for the gas phase, which means that the impact led finally to a certain amount of boil-off. This was also expected since the piston brought an external amount of energy to the fluid. This added boil-off could also be considered as the price for a sloshing pressure reduction…

SCALING GAS POCKET PRESSURES

As it has been done in Bogaert et al. (2010) and Kimmoun et al. (2010) with Bagnold's model, it is very tempting to use the extended model at two different scales in order to compare pressures obtained in gas

pockets at both scales. Lafeber et al. (2012) showed that this approach is perfectly relevant by comparing directly two couples of Froude-similar breaking waves at two different scales.

Figure 14 displays Bagnold's curve ${P_{Bag}}^*{}_{max}(S)$ (in red) together with ${P_g}^*{}_{max}(S)$, the maximum dimensionless pressure versus the impact number S obtained with the extended model (in blue), considering initial conditions corresponding to methane at thermodynamic equilibrium at atmospheric pressure ($T_0^g = T_0^l = 111$ K, $P_0 \approx 100$ kPa), values of Onsager's coefficients derived from kinetic theory of gases ($L_{qq} = 10^9$ kg K s^{-3} and $L_{\mu\mu} = 100$ mol^2 K J^{-1} s^{-1}m^{-2}) and the initial gas volume fraction set to $\nu_0 = 0.1$.

As shown in **Figure 11** (right), the values of L_{qq} and $L_{\mu\mu}$ are not known precisely for methane but have a large influence on the resulting maximum pressure in the gas chamber whatever the impact number S. Initial gas fraction is also not precisely determined but has a large influence, as shown in **Figure 12**. Therefore, the extended Bagnold's curve taking care of phase transition for methane, displayed in **Figure 14** is also uncertain. Anyway, it must lie below Bagnold's curve but how far from it is still an open question.

Therefore, the following must be considered as an exercice, which should be updated when confirmed data are available to feed the model.

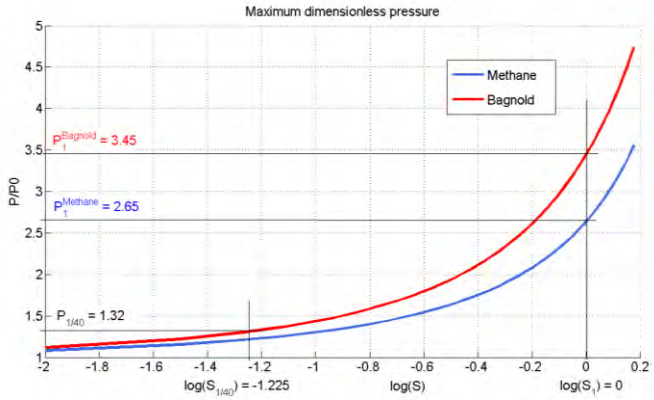

Figure 14 – Maximum dimensionless pressures obtained with Bagnold's model (red) and with the extended Bagnold's model for methane (blue) vs. impact number S for initial conditions corresponding to methane - $T_0^g = T_0^l = 111$ K, $P_0 \approx 100$ kPa, $L_{qq} = 109$ kg K s^{-3}, $L_{\mu\mu} = 100$ mol^2 K J^{-1} s^{-1}m^{-2} and $\nu_0 = 0.1$.

Let's consider a sloshing impact with a gas pocket entrapment obtained at model scale 1/λ during sloshing model tests with water and the Froude-similar impact at full scale with methane, initially in thermodynamic equilibrium at atmospheric pressure.

Bagnold's model with red curve of **Figure 14** is relevant for describing the gas pocket behavior without phase transition at small scale. Blue curve of **Figure 14** is assumed to be relevant for describing the gas pocket behavior with methane at full scale.

The pressures at full scale ${P_g}^{(1)}$ can be derived simply from the pressures at small scale ${P_g}^{(1/\lambda)}$ by the following approach, illustrated in **Figure 14** for λ=40, which corresponds to the usual scale for sloshing model tests in GTT.

For a given pressure ${P_g}^{(1/\lambda)}$, can be deduced the corresponding value of the impact number at small scale $S^{(1/\lambda)}$. As the inflow conditions are Froude-similar at both scales, there is a relation between the impact numbers at both scales : $S^{(1)} = \lambda\,\mu\,S^{(1/\lambda)}$, where 1/μ is the mass scale for liquids $\frac{1}{\mu} = \frac{\rho_l^{(1/\lambda)}}{\rho_l^{(1)}}$, assuming that the mass piston is obtained at both scales by scaled lengths of liquids. ${P_g}^{(1)}$ can now be simply derived from $S^{(1)}$ and the blue curve.

Results displayed in **Figure 14** shows that a *dynamic* pressure *(P-P$_0$)* of 0.3 bar measured in a gas pocket at model scale would correspond to a dynamic pressure of 2.45 bars at full scale without phase transition but only to 1.65 bars with phase transition. The magnitude of the mitigation is therefore 33%. Applying wrongly a Froude similarity to the gas pocket pressure would have led to a pressure of 5.4 bars.

Figure 15 shows pressures at full scale as a function of pressures at small scale following the previous approach.

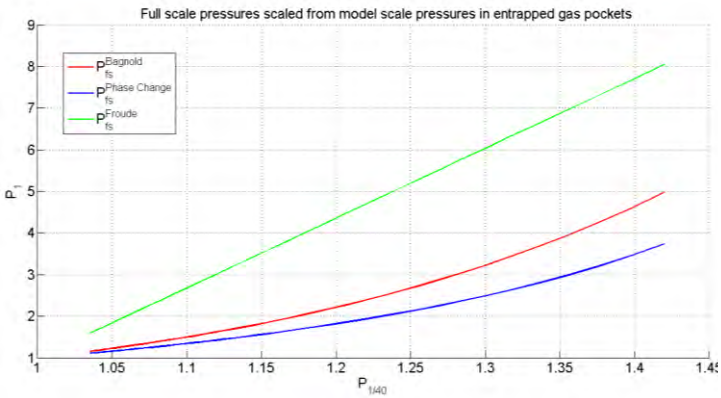

Figure 15 – Pressures at full scale vs. pressure at model scale for gas pockets - Froude scaling (green), Bagnold's model (red), extended Bagnold's model (blue) for initial conditions corresponding to methane $T_0^g = T_0^l = 111$ K, $P_0 \approx 100$ kPa, $L_{qq} = 10^9$ kg K s^{-3} $L_{\mu\mu} = 100$ mol^2 K J^{-1} s^{-1}m^{-2} and $\nu_0 = 0.1$.

CONCLUSIONS

An extension of Bagnold's piston model has been developed in order to include the energy and mass transfers occurring between a liquid and its vapor during a liquid impact with a vapor pocket entrapped, when the two phases are close to a thermodynamic equilibrium. The objective is to better understand the role of phase transition during sloshing impacts on board membrane LNG carriers.

The model is based on Non-Equilibrium Thermodynamics (NET) and allows to simulate the relaxation phase for a pure fluid in between initial unbalanced thermodynamic conditions and the final equilibrium along the phase boundary. It is a more sophisticated model than the model presented in Braeunig et al., (2010) but nevertheless also more robust, likely because it includes more physics (energy conservation).

The model allows to study the thermodynamic relaxation for a large range of initial conditions, including different initial relative locations in the (P, T) diagram for the liquid and gas phases with regard to the saturation curve and different liquid volume fractions.

The model uses the three Onsager's transport coefficients. They are supposed to evolve slightly with the thermodynamic parameters. After a sensitivity study for several initial conditions with a complete determination of Onsager's coefficients based on the kinetic theory of gases, the range of variation of each coefficient has been considered as sufficiently narrow to keep them constant without much loss of accuracy. Moreover, the coupling coefficient has been neglected, considering its influence as insignificant. Nevertheless the values for the two remaining constants are controversial and the large range

offered by experimental or theoretical results for these values brings a large uncertainty on the fluid properties used in the model.

A dimensionless version of the model has been developed and implemented under Matlab. Impact number *S*, which is characteristic of the impact strength and governs the simple Bagnold's model, is also one of the dimensionless numbers of the extended problem. Other dimensionless numbers are related to thermo-dynamic properties of the fluid (thermal capacities, latent heat), but also characteristic times for respectively energy transfer and mass transfer.

When these times are too large for any energy or mass transfer to be possible during the short impact duration, the model tends naturally towards Bagnold's solution.

Whatever the exact values of the Onsager's coefficients in the whole reasonable range for them, phase transition always leads to a reduction of the maximum pressure in the gas pocket and to oscillation damping, according to the model proposed. Depending on the fluid properties (including Onsager's coefficients) and initial conditions, a double „resonance' of the mitigation process is possible, when the characteristic times of the energy and mass transfers are well fitted to the impact duration. The mitigation process is also significantly favored by a large presence of liquid around the entrapped gas.

Provided that the liquid fraction is high, time traces of the gas pocket pressure, as calculated by the model, are very much alike those obtained during sloshing model tests with water and vapor (see **Figure 2** extracted from Maillard et al., 2009), with almost complete disappearance of the pressure oscillations in all gas pockets. Furthermore, the reduction of statistical pressures that is reported by Maillard, when comparing sloshing tests with and without possible phase transition but with the same density ratio between gas and liquid, is perfectly understandable by the mitigation process shown by Bagnold's extended model.

The strength of such surrogate models based on Ordinary Differential Equations (ODE) had already been demonstrated in Bogaert et al. (2010) or Kimmoun et al. (2010) by giving a convincing explanation to the different experimental scaling factors obtained when comparing wave impact gas pocket pressures and oscillation frequencies at different scales. Here, the extended Bagnod's model was also able to explain additional experimental trends observed for wave impact gas pocket pressures when phase transition is involved.

Using this model for scaling gas pocket pressures from sloshing model test scale to full LNG tank scale is tempting. As the impact numbers at both scales are simply related by a factor which is the product of the geometrical and the liquid density scales, deriving a scaled pressure from a model scale pressure is trivial using the relevant ${P_g}^*{}_{max}(S)$ curve related to methane, obtained from the model. Unfortunately, as there is a large uncertainty on the thermodynamic properties as well as the liquid fraction to introduce into the model, there is also a large uncertainty on the real shape of ${P_g}^*{}_{max}(S)$ curve. Nevertheless the general mitigation process brought by phase transition leads thus to exhibit an additional safety margin, the magnitude of which only is uncertain.

Although the authors are convinced of the generality of the mitigation process due to phase transition, they must admit that, up to now, it lies only on a theoretical model based on strong assumptions (pure fluid, perfect gas, constant temperature in each phase) and on sloshing model tests with water and vapor, also with strong restrictions (only high fills) and not especially designed to address the phase transition influence. Additional experimental data would be therefore very much welcome to confirm the trend. The best would be to perform wave impact tests in a small flume lying in a pressure vessel, in order to enable the use of water in equilibrium with its vapor, but also to use other kinds of non condensable gases for comparison. Wave impact tests would be more suitable than sloshing model tests for such a purpose as they allow to accurately obtain repeatable shapes of breaking waves in front of the impacted wall and therefore accurately repeatable pressures measured within the entrapped gas pockets.

The extended Bagnold's piston model to phase transition deserves some further extensions. Among them, the introduction of a thermal gradient along the piston course axis, the possibility to take into account phase transition within the bulk of both phases far from the existing interface and the introduction of external thermal exchange, seem to be the most relevant.

More generally, the development and use of more and more sophisticated surrogate models (ODE or 1D Partial Differential Equations (PDE)), in addition to dedicated experiments (see Lafeber et al., 2012) and numerical simulations (see Guilcher et al., 2012), remains a research objective of GTT for a more and more direct approach to address the scaling issues generated by the biased gas and liquid properties during model tests. Bagnold's model can be considered as the most simple base, from which are introduced many extensions such as : escaping of gas, liquid compressibility, aeration, fluid-structure interactions, etc, as well as phase transition, in order to eventually cover the complete impact chart possibilities described in **Figure 1**.

As the designer of the membrane containment systems for LNG tanks, the main objective of GTT remains the safety of its solutions onboard LNG ships. It has to be checked carefully whether the phase transition could be, in certain conditions to be determined, an amplifying phenomenon of the sloshing impact pressures. Up to now, through the sloshing model tests with water and vapor and through results of the extended Bagnold's model, the phase transition looks as a mitigating effect that is not taken into account during the sloshing model tests, therefore adding implicitly a safety factor to the tests results.

The mechanism described with this model leads finally at each initial compression of the piston to evaporation, whatever the way to reach the new state of equilibrium. This is intuitively normal as external energy is brought by the piston to the fluid. Transposed to LNG carriers, this would mean that at each sloshing impact involving a gas pocket, a certain amount of boil-off is generated, which is the price for a reduction of the induced pressure. Therefore, this anti-sloshing mechanism is likely responsible for a good share in the increased boil-off observed by the operators at each loaded journey of LNG ships with harsh sea conditions. It should be comforting for them to consider now that this inconvenience is not a pure waste.

REFERENCES

Ancellin, M, (2011), "*Modélisation macroscopique et simulation numérique du retour à l'équilibre liquide-vapeur*", Publication du CMLA 2012-05. http://tinyurl.com/Ancellin2011

Badam, V.K., Kumar, V., Durst, F., Danov, K., (2007), "*Experimental and theoretical investigations on interfacial temperature jumps during evaporation*", Experimental Thermal and Fluid Science, 32(1):276-292, 2007.

Bagnold, R., (1939), *"Interim report on wave-pressure research"*, J. Inst. Civil Eng. 12: 201–226.

Bedeaux, D., Kjelstrup, S., (1999), *"Transfer coefficients for evaporation"*, Physica A: Statistical Mechanics and its Applications, 270: 413-426, 1999.

Bogaert, H., Brosset, L., Léonard, S., Kaminski, M., (2010). *"Sloshing and scaling: results from Sloshel project"*, 20th (2010) Int. Offshore and

Polar Eng. Conf., Beijing, China, ISOPE.

Braeunig, J.-P., Brosset, L., Dias, F., Ghidaglia, (2009), "*Phenomenological study of liquid impacts through 2D compressible two-fluid numerical simulations*", 19th (2009) Int. Offshore and Polar Eng. Conf., Osaka, Japan, ISOPE.

Braeunig, J.P., Brosset, L., Dias, F., Ghidaglia, J.M., (2010), *"On the effect of phase transition on impact pressures due to sloshing"*, 20th (2010) Int. Offshore and Polar Eng. Conf., Beijing, China, ISOPE.

Brosset, L., Lafeber, W., Bogaert, H., Marhem, M., Carden, P., Maguire, J. (2011) "*A Mark III Panel Subjected to a Flip-through Wave Impact: Results from the Sloshel Project*", 21st (2011) Int. Offshore and Polar Eng. Conf., Maui, (HI), USA, ISOPE.

Couty, N., Brosset, L. (2000), "*3D numerical simulation of sloshing impacts including fluid-structure interaction*", 13th International Conference on Ship and Shipping Research (NAV'2000), 19-22 Sept. 2000, Venice, Italy.

Faltinsen, O.M., Timokha , A.N. (2009), "*Sloshing*", Cambridge University Press.

Fang, G., Ward, C.A., (1999), "*Temperature measured close to the interface of an evaporating liquid*", Physical Review E, 59(1) : 417, 1999.

Gervaise, E., de Sèze, P.E., Maillard, S., (2009), *"Reliability-based methodology for sloshing assessment of membrane LNG vessels"*, 19th (2009) Int. Offshore and Polar Eng. Conf., Osaka, Japan, ISOPE.

Guilcher, P.M., Brosset, L., Jacquin, E., Le Touzé, D., (2012), "*Simulations of breaking wave impacts on a Mark III containment system for LNG carriers with a two phase fluid-structure SPH model",* 22th (2012) Int. Offshore and Polar Eng. Conf., Rhodos, Greece, ISOPE.

Kimmoun, O., Ratouis, A., Brosset, L. (2010), *"Sloshing and scaling: experimental study in a wave canal at two different scales"*, 20th (2010) Int. Offshore and Polar Eng. Conf., Beijing, China, ISOPE.

Lafeber, W., Brosset, L., Bogaert, (2012), "*Elementary Loading Processes (ELP) involved in breaking wave impacts: findings from the Sloshel project*", 22th (2012) Int. Offshore and Polar Eng. Conf., Rhodos, Greece, ISOPE.

Lafeber, W., Brosset, L., Bogaert, (2012), "*Comparison of wave impact tests at large and full scale: results from the Sloshel project*", 22th (2012) Int. Offshore and Polar Eng. Conf., Rhodos, Greece, ISOPE.

Lebon, G., Jou, D., Casas-Vázquez, J. (2008), *Understanding Non-equilibrium Thermodynamics: Foundations, Applications, Frontiers*, Springer-Verlag, Berlin

Maillard, S., Brosset, L., (2009), *"Influence of Density Ratios between liquid and gas on sloshing model test results"*, 19th (2009) Int. Offshore and Polar Eng. Conf., Osaka, Japan, ISOPE.

Zhao, R.; Faltinsen, O. M., (1993). "*Water entry of two-dimensional bodies*", Journal of Fluid Mechanics, vol. 246, p.593-612.